Bubbling transition to spatial mode excitation in an extended dynamical system

J.D. Szezech Jr. [a], S.R. Lopes [a], R.L. Viana [a,*], I.L. Caldas [b]

[a] Departamento de Física, Universidade Federal do Paraná, Caixa Postal 19044, 81531-990, Curitiba, Paraná, Brazil
[b] Instituto de Física, Universidade de São Paulo, 05315-970, São Paulo, São Paulo, Brazil

ABSTRACT

We investigated the transition to spatio-temporal chaos in spatially extended nonlinear dynamical systems possessing an invariant subspace with a low-dimensional attractor. When the latter is chaotic and the subspace is transversely stable we have a spatially homogeneous state only. The onset of spatio-temporal chaos, i.e. the excitation of spatially inhomogeneous modes, occur through the loss of transversal stability of some unstable periodic orbit embedded in the chaotic attractor lying in the invariant subspace. This is a bubbling transition, since there is a switching between spatially homogeneous and nonhomogeneous states with statistical properties of on–off intermittency. Hence the onset of spatio-temporal chaos depends critically both on the existence of a chaotic attractor in the invariant subspace and its being transversely stable or unstable.

© 2008 Elsevier B.V. All rights reserved.

1. Introduction

A theoretical description of turbulence in fluids and plasmas has been one of the key problems in theoretical physics during the last decades [1]. While the problem of fully-developed turbulence has a comprehensive description (Kolmogorov 1941 theory) which matches experimental evidence [2], the onset of turbulence is a far more difficult question, which dates back to early Landau theory [3] and is by now not completely solved yet. An extensively studied description for the onset of turbulence is a sequence of Hopf bifurcations yielding a chaotic attractor in the system phase space [4]. While this route has been verified in many systems of physical interest [5], there are situations for which the onset of turbulence is thought to be caused by other mechanisms [6].

One of the stumbling blocks on investigating turbulence in fluids and plasmas is the large number of degrees of freedom necessary to describe the energy flow from large to small-scale structures [7]. Hence a simplified theoretical description for fluids and plasmas is to describe them by extended dynamical systems in which there is energy flow from temporal to spatial degrees of freedom, the latter being represented by Fourier modes in a reciprocal phase space. In fact, given our thorough understanding of purely temporal chaotic behavior (as reviewed, for example, in Ref. [8]) we might well ask to what extent it is possible to use this expertise to interpret the onset of spatio-temporal chaos in terms

of the excitation of spatial modes drawing energy from a purely chaotic temporal mode [9]. This mechanism, whenever it occurs in a given spatially extended dynamical system, provides a transition scenario which can shed more light on the general problem of the onset of turbulence in fluids and plasmas.

Hence, instead of dealing directly with turbulence we shall focus on a more limited concept, which is spatio-temporal chaos, characterized by: (a) chaotic temporal dynamics; (b) decaying spatial correlations [10]. A spatially homogeneous and temporally chaotic system will be taken as the reference state to which we characterize the onset of spatio-temporal chaos. The latter occurs when part of the energy of the purely temporal mode is relayed to a spatial mode, causing its excitation through a nonlinear mode conversion. We emphasize that such spatial mode excitation is only possible if temporal chaos is present in the spatially homogeneous state, which acts as a stochastic pump to excite more and more spatial modes [11]. The distribution of the energy among these modes is thus a quantitative evaluation of the spatio-temporal chaos present in the system.

In this paper we consider the expansion in discrete spatial modes in a reciprocal (Fourier) lattice, by using a pseudo-spectral procedure [12]. From the mathematical point of view we work in a finite-dimensional (Fourier) phase space defined by the modes retained in the expansion. The spatially homogeneous state thus defines a low-dimensional homogeneous subspace, the transversal directions to which being the spatial modes to be excited after the onset of spatio-temporal chaos [13]. The latter will occur when this homogeneous subspace loses transversal stability, a mechanism not directly related with the breakup of some high-dimensional torus [14].

* Corresponding author.
  E-mail address: viana@fisica.ufpr.br (R.L. Viana).

From the discussion above it follows that there must be a chaotic attractor embedded in the homogeneous subspace for this transition to occur. This chaotic attractor, on its hand, has an infinite number of unstable periodic orbits forming the topological tapestry which supports the ergodic measure of the trajectories on the attractor [15]. Although the large dimensionality of the phase space prevents us from identifying the specific periodic orbit which loses transversal stability, we can resort to numerical diagnostics in order to identify this transition.

Moreover, since only a measure zero set of unstable periodic orbits lose transversal stability there will remain a dense set of transversely stable orbits embedded in the chaotic attractor [16]. As a result, just after the transition to spatio-temporal chaos a trajectory outside the homogeneous subspace exhibits the bubbling phenomenon: it remains near the homogeneous state (homogeneous chaotic behavior) for some time, until it bursts out of it provoking the excitation of some spatial mode [17]. In fact, the statistical properties of this bubbling transition belong to the same category as of low-dimensional systems undergoing the so-called on–off intermittency [32]. In this paper we explore the similarities and differences between low-dimensional chaotic systems and high-dimensional spatio-temporal systems with respect to this bubbling transition.

We claim that the bubbling transition to spatial mode excitation is a typical scenario in spatially extended dynamical systems, since the pre-conditions for it are sufficiently general: (i) the existence of a spatially homogeneous and temporally chaotic state; (ii) the loss of transversal stability of some low-period orbit embedded in the chaotic attractor of the spatially homogeneous state. In order to support this claim, we present numerical results for three nonlinearly interacting and dispersive waves in one spatial dimension suffering Laplacian diffusion. Such systems occur in a plethora of problems in fluid dynamics [18], plasma physics [19] and nonlinear optics [20]. Three-wave interactions are mathematically described by a system of coupled-mode nonlinear partial differential equations which exhibit complex behavior [21]. The nonlinear three-wave model describes the exchange of energy among a high-frequency (parent) wave and its sideband (daughters) with quadratic interactions, as well as with a spatial diffusion term. This system is known to present a rich spatio-temporal behavior, including weak turbulence [22, 23]. While we consider a temporally monochromatic and spatially polychromatic spectrum, a related situation but with temporally polychromatic and spatially monochromatic spectrum has been investigated in Ref. [24].

The rest of this paper is organized as follows: Section 2 describes the three-wave interacting model and the Fourier mode expansion we make in order to work in a reciprocal lattice. Section 3 considers the spatio-temporal dynamics exhibited by this model, focusing on the nonlinear excitation of spatial modes. Section 4 describes the onset of spatio-temporal chaos in the three-wave model through loss of transversal stability of the spatially homogeneous state undergoing temporally chaotic evolution. Section 5 treats the bubbling phenomenon following the transition to spatio-temporal chaos and its similarities with on–off intermittency. Section 6 is devoted to discussing the role of diffusion on the spatial mode excitation and the nonlinear transfer of energy among spatial modes. Our conclusions appear in the last section.

2. The model

Let the complex amplitudes A_α, $\alpha = 1, 2, 3$, describe three dispersive monochromatic waves propagating along the x-direction. Their wave numbers and frequencies must satisfy matching conditions for the triplet,

$$\mathbf{k}_3 = \mathbf{k}_1 + \mathbf{k}_2, \tag{1}$$

$$\Omega_{\mathbf{k}_3} = \Omega_{\mathbf{k}_1} - \Omega_{\mathbf{k}_2} - \delta, \tag{2}$$

where δ is a small frequency mismatch, which has been introduced because, even for perfectly matched wave vectors, the respective frequencies obtained from the linear dispersion relations may not be likewise matched. This effect occurs quite often in laser–plasma interactions, where it can enhance the linear growth rate [23]. For the same reasoning wave vector mismatches could also be taken into account, but since it is formally equivalent to frequency mismatch it suffices to analyze the latter.

Each wave has a constant group velocity $v_{g\alpha} = \mathrm{d}\Omega_{\mathbf{k}_\alpha}/\mathrm{d}k_\alpha$, given by its linear dispersion relation, and we shall assume in this paper that $v_{g2} > v_{g1} > v_{g3}$. This is consistent with a scenario where $A_1(x, t)$ stands for the parent wave amplitude, $A_2(x, t)$ and $A_3(x, t)$ being the corresponding quantities for the faster and slower daughter waves, respectively [21]. In the case of nonlinear wave interactions in nonmagnetized plasmas, A_1 may stand, for example, for a transverse electromagnetic wave, A_2 a ion-acoustic wave, and A_3 is a Langmuir wave (anti-Stokes mode) [19].

We also suppose that the nonlinearities present in the wave interactions are sufficiently weak, such that only quadratic terms in the wave amplitudes need to be considered. In this case the three-wave system can be described by the following Hamiltonian density [23]

$$\mathcal{H} = -A_1 A_2^* A_3^* + A_1^* A_2 A_3 + \mathrm{i}\delta \, |A_3|^2 - \sum_{\alpha=1}^{3} v_{g\alpha} A_\alpha^* \frac{\partial A_\alpha}{\partial x}, \tag{3}$$

such that the equations governing the spatio-temporal dynamics of the system are obtained from

$$\frac{\partial A_\alpha}{\partial t} = \frac{\delta H}{\delta A_\alpha^*}, \tag{4}$$

$$\frac{\partial A_\alpha^*}{\partial t} = -\frac{\delta H}{\delta A_\alpha}, \tag{5}$$

where $H = \int \mathrm{d}x \mathcal{H}$ and the functional derivative is

$$\frac{\delta}{\delta A_\alpha} \equiv \frac{\partial}{\partial A_\alpha} - \frac{\partial}{\partial x} \frac{\partial}{\partial \left(\frac{\partial A_\alpha}{\partial x}\right)}. \tag{6}$$

Since the Hamiltonian H does not depend explicitly on time it is a conserved quantity. We can introduce fenomenologically dissipation by adding growth and decay rates: the coefficients $v_1 > 0$ and $v_{2,3} < 0$ represent energy injection (through wave 1) and dissipation (through waves 2 and 3), respectively. This sign convention follows from a linear analysis in which the parent wave is supposed to grow exponentially with time, whereas the daughter waves are expected to decay exponentially in each cycle. Diffusion is also introduced by a Laplacian term in the parent wave, which provides a cutoff in the linear wave growth, being essential to nonlinear saturation [22].

With such modifications, the equations governing the dynamics of the resonant three-wave interaction are [21,22]

$$\frac{\partial A_1}{\partial t} + v_{g1} \frac{\partial A_1}{\partial x} = A_2 A_3 + v_1 A_1 + D \frac{\partial^2 A_1}{\partial x^2}, \tag{7}$$

$$\frac{\partial A_2}{\partial t} + v_{g2} \frac{\partial A_2}{\partial x} = -A_1 A_3^* + v_2 A_2, \tag{8}$$

$$\frac{\partial A_3}{\partial t} + v_{g3} \frac{\partial A_3}{\partial x} = \mathrm{i}\delta A_3 - A_1 A_2^* + v_3 A_3, \tag{9}$$

where D is a diffusion coefficient.

In the configuration we have chosen, a parent wave has a positive linear growth rate and pumps energy to the daughter waves. We kept the group velocities, frequency mismatch, and diffusion coefficient at fixed values: $v_{g1} = 0.0$, $v_{g2} = 1.0$, $v_{g3} = -1.0$, $\delta = 0.1$, and $D = 1.0$, respectively. This parameter choice
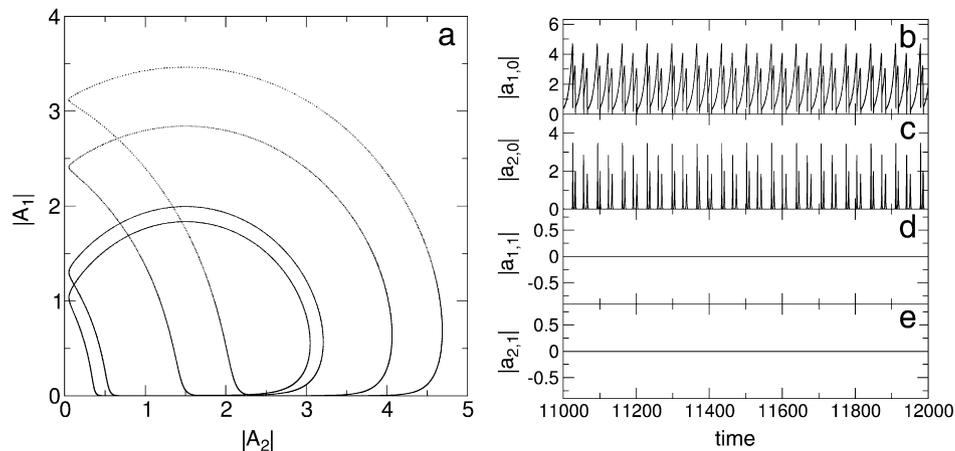
Fig. 1. (a) Projection of the low-dimensional attractor in the $|A_1|$ vs. $|A_2|$ section of the phase space when $\nu_1 = 0.1$, $\nu_{2,3} = -1.5$. (b)–(e) Time evolution of the (Fourier) mode amplitudes $|a_{\alpha,n}|$ for $\alpha = 1, 2$ and $n = 0, 1$.

would correspond, in the treatment given by Ref. [21], to the so-called solitonic regime. The growth rate will be often kept fixed as $\nu_1 = 0.1$, and the decay rate $\nu_2 = \nu_3$ are negative and will be taken as equal for simplicity. The latter shall be the tunable parameter in the numerical simulations to be shown hereafter. Eqs. (7)–(9) were numerically integrated by a pseudo-spectral method using a fixed number N of modes in Fourier space (for a one-dimensional box of length L with periodic boundary conditions) [25]

$$A_\alpha(x, t) = \sum_{n=-(N/2)+1}^{N/2} |a_{\alpha,n}(t)| \exp\left\{ i\left[\kappa_{\alpha,n} x + \phi_{\alpha,n}(t) \right] \right\},$$
$$(\alpha = 1, 2, 3), \tag{10}$$

where $a_{\alpha,n}(t)$ is the time-dependent Fourier coefficient corresponding to the mode number $\kappa_{\alpha,n} = 2\pi n/L$, and whose evolution is governed by a system of $6N$ coupled ordinary differential equations, since the mode amplitudes themselves are complex variables. We used a box length $L = 2\pi/\kappa_{1,1} = 2\pi/0.89$. The initial conditions are chosen as $F_{1,0}(0) = 0.500 + i0.000$, and $F_{2,\pm1}(0) = 0.001 + i0.001$, where

$$F_{\alpha,n}(t) = a_{\alpha,n}(t) e^{i\phi_{\alpha,n}(t)}, \tag{11}$$

all the other modes being set to zero.

3. Nonlinear excitation of spatial modes

The $\kappa_{\alpha,0}$ modes do not contain the spatial variable and thus reflects only the temporal dynamics of the wave interaction process. We can put this observation in the context of the $6N$-dimensional phase space comprised by the Fourier modes retained in the expansion above. The modes with $\kappa_{\alpha,0} \neq 0$ and $\kappa_{\alpha,i} = 0$, $(i \neq 0)$, correspond to a purely temporal dynamics (periodic, quasi-periodic, or chaotic) and a spatially homogeneous state. For the case $\nu_2 = \nu_3$, and thanks to a phase conjugacy in the resonant three-wave equations, it is possible to show that the spatially homogeneous states define a 3-dimensional invariant subspace of the full phase space of the system, which we will hereafter refer to as the homogeneous manifold $\mathcal{M}$ [8]. This subspace is invariant in the sense that, once an initial condition is placed there, the ensuing trajectory remains in $\mathcal{M}$ for all further times under the dynamics generated by the $\kappa_{\alpha,0}$ modes. Accordingly, the spatially inhomogeneous modes $\kappa_{\alpha,n}$ are related to directions transversal to $\mathcal{M}$.

We plotted in Fig. 1(a) a two-dimensional projection of the homogeneous subspace by considering the behavior of the

amplitudes $|A_1|$ and $|A_2|$ as a function of time and entirely contained in the homogeneous manifold $\mathcal{M}$. In this case only the purely temporal modes are excited, as exemplified by the time series of the $|a_{1,0}|$ and $|a_{2,0}|$ modes (Fig. 1(b) and (c), respectively). The latter are clearly periodic, what is also reflected in the attractor projection (Fig. 1(a)), which is a stable period-4 orbit. Spatial modes representing excursions off the homogeneous manifold do not exist, however, since the amplitudes $|a_{1,1}|$ and $|a_{2,1}|$ are equal to zero as well as higher spatial modes (Fig. 1(d) and (e), respectively).

One of the main points of this work is that the excitation of such spatial modes requires chaotic behavior in the homogeneous manifold. However, the converse is not necessarily true, as illustrated by Fig. 2(a), where we consider the system dynamics is temporally chaotic but inhomogeneous spatial modes $\kappa_{\alpha,n}$ remain inactive. From Fig. 2(b) we infer that the behavior of the mode $|a_{1,0}|$ is essentially that expected from the parent wave amplitude in the absence of spatial diffusion: the mode amplitude initially grows exponentially with the linear growth rate ν_1, but it eventually saturates due to the quadratic terms in the right hand side of Eq. (7).

After reaching a maximum value the parent wave imparts its energy to the daughter waves, which have noise-level amplitudes during the linear growth of the parent wave, as shown by the time evolution of the $|a_{2,0}|$ mode (Fig. 2(c)), the same conclusion holding for $|a_{3,0}|$. The daughter waves present impulsive temporal dynamics, as a result of the nonlinear energy transfer from/to the parent wave. As the $|a_{1,0}|$ mode amplitude decreases abruptly the daughter amplitudes $|a_{2,0}|$ and $|a_{3,0}|$ grow and decay likewise fast in the form of spikes. After such a spike the daughter modes give energy back to the parent wave, which grows again comprising the basic interaction process. Depending on the values of the parameter $\nu_{2,3}$ both the maximum wave amplitudes and the interspike intervals vary chaotically with time [26]. Yet according to Fig. 2(d) and (e), respectively, the mode amplitudes $|a_{1,1}|$ and $|a_{2,1}|$ vanish in the same fashion as before.

When the dissipation increases further on, while the dynamics of homogeneous modes remain chaotic (Fig. 3(a)), spatial modes become excited. The linear growth and nonlinear decay of the parent wave mode $|a_{1,0}|$ is followed by spikes both in the temporal ($|a_{2,0}|$) and spatial modes ($|a_{1,1}|$ and $|a_{2,1}|$) (Fig. 3(b)). The spatial mode amplitudes spikes are synchronized with the temporal mode spikes, showing that the overall energy pump mechanism is still the chaotic behavior of the parent wave in the homogeneous manifold. The inactivity of spatial modes observed in the previous cases can be interpreted by regarding
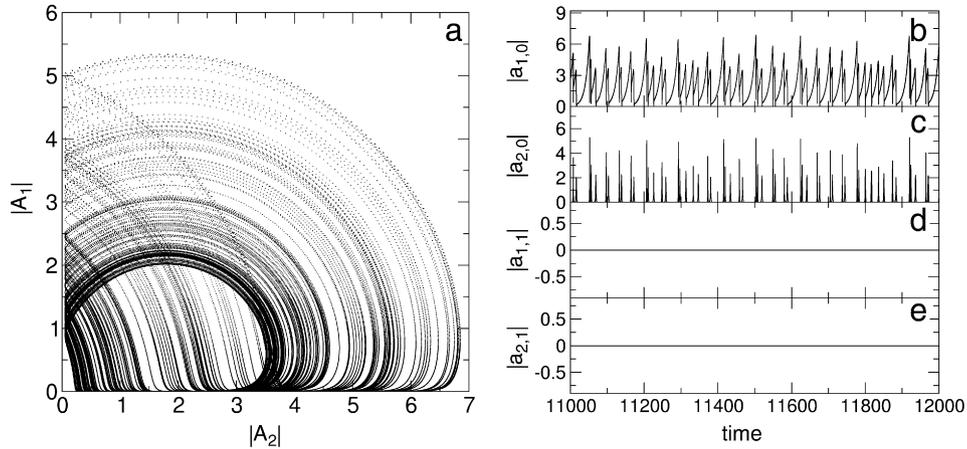
Fig. 2. (a) Projection of the low-dimensional attractor in the $|A_1|$ vs. $|A_2|$ section of the phase space when $\nu_{2,3} = -1.8$. (b)–(e) Time evolution of the (Fourier) mode amplitudes $|a_{\alpha,n}|$ for $\alpha = 1, 2$ and $n = 0, 1$.
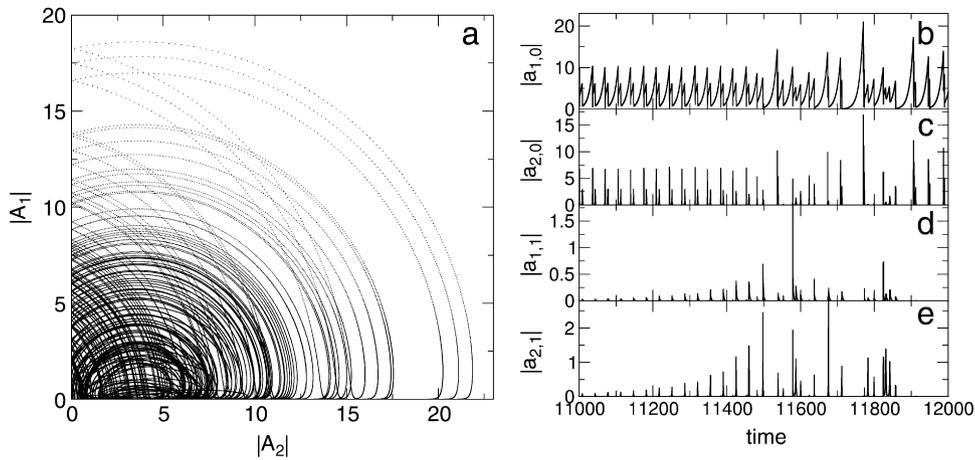

Fig. 3. (a) Projection of the spatio-temporal attractor in the $|A_1|$ vs. $|A_2|$ section of the phase space when $\nu_{2,3} = -3.6$. (b)–(e) Time evolution of the (Fourier) mode amplitudes $|a_{\alpha,n}|$ for $\alpha = 1, 2$ and $n = 0, 1$.

the spatial modes as being transversely stable with respect to the homogeneous manifold [25]. In other words, any perturbation bringing the system outside the homogeneous manifold along some transversal direction would fade out at an exponential rate to $\mathcal{M}$. In the case of Fig. 3, however, the spatial modes have lost transversal stability and the wave energy is distributed along temporal and spatial modes, provoking inhomogeneous spatial patterns. We emphasize that it is essential that the dynamics in the homogeneous manifold be chaotic in order to provide a pump mechanism to feed energy to the spatial modes.

Another view of the dynamics in the homogeneous manifold comes from regarding the mode amplitudes $|a_{\alpha,n}|$ as coupled oscillators *real space*, in such a way that a purely chaotic behavior (i.e. without spatial mode excitation) would correspond to a spatially synchronized state. In order to do this we must consider the wave amplitudes at a fixed point x_i from the reciprocal lattice of the point grid in Fourier space, denoted as $|A_\alpha(i, t)| = |A_\alpha(x = x_i, t)|$. Accordingly there are out of N points in the reciprocal lattice, such that a completely synchronized state is [27]

$$A_\alpha(1, t) = A_\alpha(2, t) = \cdots = A_\alpha(N, t), \qquad (12)$$

for all times, and which can be put into evidence, for example, by drawing return plots of $|A_\alpha(i, t)|$ *versus* $|A_\alpha(j, t)|$, where x_i and x_j are two distinct points. Considering a fixed x_i we depicted in Fig. 4(a) and (b) the superposition of N such return plots, for values

of the control parameter for which there is and there is not a synchronized state, respectively. We emphasize that the former case refers to dynamics restricted to the homogeneous manifold, whereas in the latter case there are spatial modes excited.

Spatio-temporal plots are also useful to distinguish these regimes, as shown in Fig. 5, where the x-values refer to a box of length $L = 2\pi/\kappa_{1,1} = 2\pi/0.89$ and periodic boundary conditions. In the vertical axis we plotted the real wave amplitude $|A_1|$ and, for the ease of visualization, we also used a color code for its values. In Fig. 5(a) the synchronized state is easily seen as the flat profiles in real space which evolve chaotically in time, as is the case when the chaotic dynamics is restricted to the homogeneous manifold. Just after the loss of transversal stability of the latter (Fig. 5(b)) the synchronized state becomes a wiggling pattern, due to the excitation of low-order spatial modes, characterizing the onset of spatio-temporal chaotic state. When the growth-decay rates are further increased (in absolute value) a larger number of spatial modes are excited, making for a weakly turbulent state of spatio-temporal chaos (Fig. 5(c)).

4. Loss of transversal stability of the homogeneous subspace

The exact dynamical mechanism underlying the loss of transversal stability of the homogeneous manifold is quite elusive since the dimensionality of the phase space is too large for a
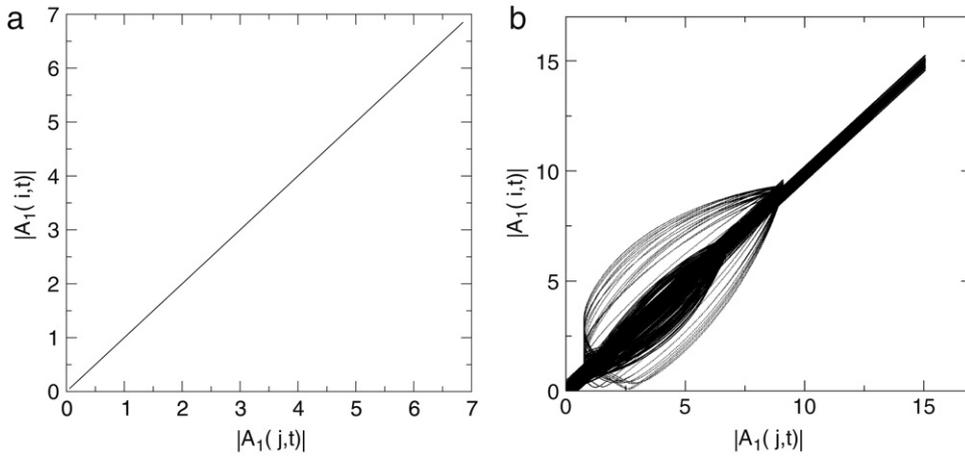
Fig. 4. Superposition of return plots of $|A_1(i, t)|$ versus $|A_1(j, t)|$, where $x_i = x_1$ and $x_j, j = 2, 3, \ldots, N$, are distinct points belonging to the reciprocal lattice in the real space. (a) $v_{2,3} = -1.8$; (b) $v_{2,3} = -3.6$.
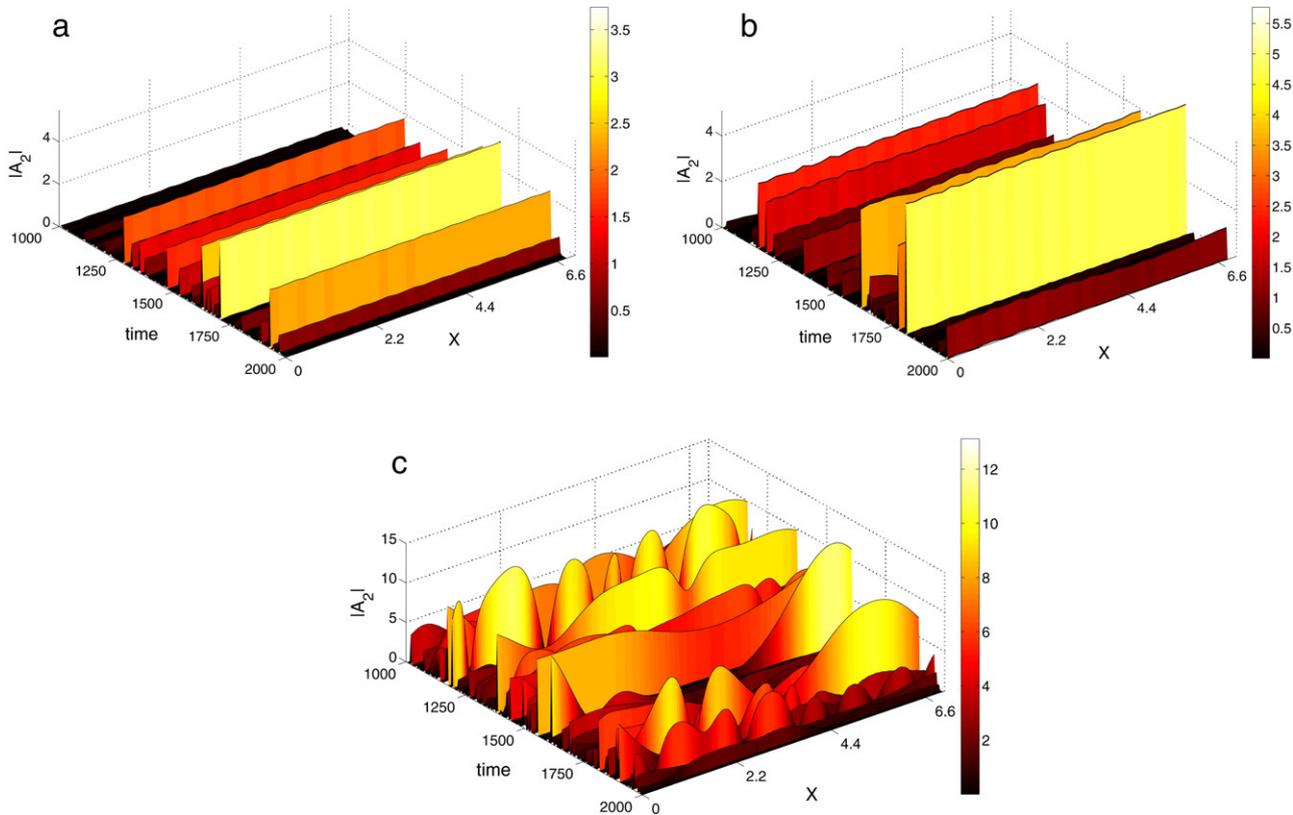

Fig. 5. (color online) Space–time plots of the real wave amplitude $|A_2|$ (also indicated by a color scale) when (a) $v_1 = 0.1$, $v_{2,3} = -1.8$; (b) $v_1 = 0.1$, $v_{2,3} = -3.6$; (c) $v_1 = 0.5$, $v_{2,3} = -7.0$. The values of x are normalized to a box of length $L = 2\pi/\kappa_{1,1} = 2\pi/0.89$ and periodic boundary conditions.

direct attack using, e.g. linear stability theory. In low-dimensional dynamical systems this mechanism has been described as a bifurcation (saddle-node, transcritical, or pitchfork) [28]. In order to do the same for our system we would need to know what orbit loses transversal stability first, and secondly to assign a normal form to the transversal dynamics related to that orbit. Since we do not have such prior knowledge, we must resort to indirect means to evidence the onset of spatially excited modes via the loss of transversal stability of the homogeneous manifold.

One such criterion lies in the observation, made at the end of the previous section, that the loss of transversal stability implies in the breakdown of the synchronized state for the coupled Fourier mode oscillators. There are many numerical diagnostics of

complete synchronization, the most appropriate in our case being the complex order parameter introduced by Kuramoto [29]

$$z_\alpha(t) = R_\alpha(t) \exp\left(i\Phi_\alpha(t)\right) \equiv \frac{1}{N} \sum_{n=-(N/2)+1}^{N/2} \exp(i\varphi_{\alpha,n}(t)), \quad (13)$$

where $R_\alpha(t)$ and $\Phi_\alpha(t)$, $\alpha = 1, 2, 3$, are the amplitude and angle, respectively, of a centroid phase vector for a one-dimensional lattice of Fourier modes with periodic boundary conditions. The phase angle is computed as

$$\varphi_{\alpha,n}(t) = \arctan\left\{\frac{\text{Im}[A_{\alpha,n}(t)]}{\text{Re}[A_{\alpha,n}(t)]}\right\}. \quad (14)$$
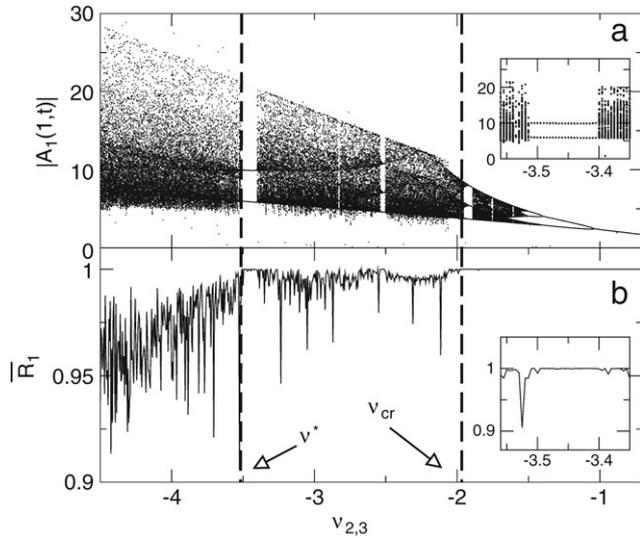
Fig. 6. (a) Bifurcation diagram for $|A_1(1, t)|$ as a function of the decay rate $\nu_{2,3}$. We denote by ν_{cr} and ν^* two particular parameter values for which there is onset of spatial activity. (b) Time-averaged order parameter for parent wave *versus* decay rate for $T = 2 \times 10^5$, after 10^4 transient iterations. The insets show the behavior in a periodic window.

The average of the order parameter magnitude

$$\overline{R_\alpha} = \lim_{T \to \infty} \frac{1}{T} \int_{n=0}^T R_\alpha(t) \mathrm{d}t, \tag{15}$$

is computed over a time interval large enough to warrant that an asymptotic state has been achieved by the system. A spatially synchronized state for all mode oscillators, signaling a purely temporal dynamics restricted to the homogeneous manifold, is characterized by $\overline{R_\alpha} = 1$, since there occurs a coherent superposition of the phase vectors with the same amplitude at each time for all discrete positions in the reciprocal lattice. The lower is the value of $\overline{R_\alpha}$, the less the spatial coherence of the system state. Accordingly the breakdown of the totally coherent state is a criterion for the appearance of spatial modes, what follows the loss of transversal stability of the homogeneous manifold.

In Fig. 6(a) and (b) we plot the bifurcation diagram for $|A_1(1, t)|$ and the average order parameter for the parent wave $\overline{R_1}$, respectively, as a function of the decay rate of the daughter waves $\nu_{2,3}$. Within the numerical accuracy the spatially homogeneous state is transversely stable for values of the decay rate higher than $\nu_{CR} \approx -1.96$, which is the value for which $\overline{R_1}$ ceases to be equal to the unity (Fig. 6(b)). The (purely temporal) dynamics in the homogeneous manifold can be either periodic or chaotic, as shown by Fig. 6(a): it starts as a period-1 orbit for small values of $|\nu_{2,3}|$ and undergoes a period-doubling cascade to chaotic bands which disappear due to a crisis and are followed by a period-3 window. The loss of transversal stability of the homogeneous manifold occurs just after a three-band chaotic attractor suffers an internal crisis and merge into a single large chaotic orbit at ν_{CR}.

The dynamics for $\nu_{2,3} < \nu_{CR}$ is chiefly chaotic, interspersed with small periodic windows, one of which is reproduced in the inset of Fig. 6(a). At the same time, most of the chaotic dynamics is associated with the excitation of spatial modes, since the order parameter magnitude there is mainly different from the unity. It is worth emphasizing, though, that chaotic behavior in the homogeneous manifold is a necessary condition for spatial modes to be excited, since we get $\overline{R_1} = 1$ whenever the dynamics goes periodic [see also the inset of Fig. 6(b) for an exploded view].

A second numerical verification of the loss of transversal stability of $\mathcal{M}$ is the computation of the Lyapunov spectrum

related to the mode dynamics in the Fourier phase space. Since each Fourier mode for the three interacting waves is a degree of freedom in this space, there are out of $6N$ Lyapunov exponents, computed using Gram–Schmidt reorthonormalization [30]. The time evolution of the three largest exponents (out of $6N$ modes considered) are depicted in Fig. 7. The homogeneous manifold is three-dimensional since waves 2 and 3 have the same values for their dissipation parameters. Henceforth, the dynamics in $\mathcal{M}$ allows just one positive Lyapunov exponent.

When the control parameter $\nu_{2,3}$ takes on values for which the dynamics in the homogeneous manifold is nonchaotic [Fig. 7(a)] the three largest exponents decay to zero as a power-law, which is an indication that they are asymptotically equal to zero. While the vanishing of the largest exponent is already expected, the other two exponents converging to zero is a further confirmation that the homogeneous manifold is transversely stable for $\nu > \nu_{CR}$. This conclusion holds even when $\lambda_1 > 0$ and the dynamics on $\mathcal{M}$ is chaotic (Fig. 7(b)). After the excitation of spatial modes (Fig. 7(c)) the two largest exponents are positive, showing that some orbits on $\mathcal{M}$ have lost transversal stability.

5. Bubbling transition to spatio-temporal chaos

The loss of transversal stability of the dynamics on the homogeneous manifold is a bubbling transition. Before the transition ($\nu_{2,3} > \nu_{CR}$) the dynamics (chaotic or nonchaotic) is confined to $\mathcal{M}$. After the transition, the orbits off but very near to $\mathcal{M}$ may experience chaotic bursts that make them depart from the homogeneous manifold due to the excitation of spatial modes (see Fig. 4(b)). Such excursions, however, are bound to turn the dynamics back to the vicinity of $\mathcal{M}$ and the orbit stays there for some time until it bursts away [17]. A representative example of the latter behavior is depicted in Fig. 8(a), in which we trace the time evolution spatial Fourier mode amplitude $|a_{2,1}|$. It jumps from zero in irregularly spaced time intervals, representing the bursts that drive the dynamics off the homogeneous manifold through nonlinear spatial mode excitation.

The periods during which there are no spatial modes excited correspond to quiescent, or laminar intervals for which the dynamics stays in the vicinity of the homogeneous manifold undergoing transient chaotic dynamics. As indicated in Fig. 8(a) we denote as τ_i the duration of an interburst interval. Since these durations vary widely it is convenient to work with a frequency distribution $P(\tau)$, such that $P(\tau)\mathrm{d}\tau$ represents the number of interburst intervals with duration between τ and $\tau + \mathrm{d}\tau$. Fig. 8(b) depicts a numerical approximation of this probability distribution obtained for two widely different values of $\nu_{2,3}$: one of them (-3.6) being close to the value $\nu^* = -3.515811$ which marks the beginning of the wide periodic window in the bifurcation diagram of Fig. 6. The other value we have taken (-2.0) is smaller but not far from the critical value ν_{CR}.

The probability distribution for the duration of inter-spike intervals scales as a power-law for small intervals and has a decreasing exponential fashion for large intervals. A nonlinear fit of the numerical results is [31]

$$P(\tau) = c_0 \tau^{-3/2} \mathrm{e}^{-c_1\tau} + c_2 \mathrm{e}^{-c_3\tau}. \tag{16}$$

The exponent $-3/2$ in the power-law part of the scaling law is a universal signature of the so-called on–off intermittency, which was formerly observed in temporal behavior of low-dimensional dynamical systems [32]. The exponential tail in Fig. 8(b) is a characteristic of noisy systems undergoing on–off bifurcation [33].

The on–off bifurcation occurs when a dynamical system, possessing an invariant subspace in which the dynamics is chaotic, is near to a bifurcation point, and for some reason the bifurcation parameter fluctuates in an irregular fashion [32]. Hence the system
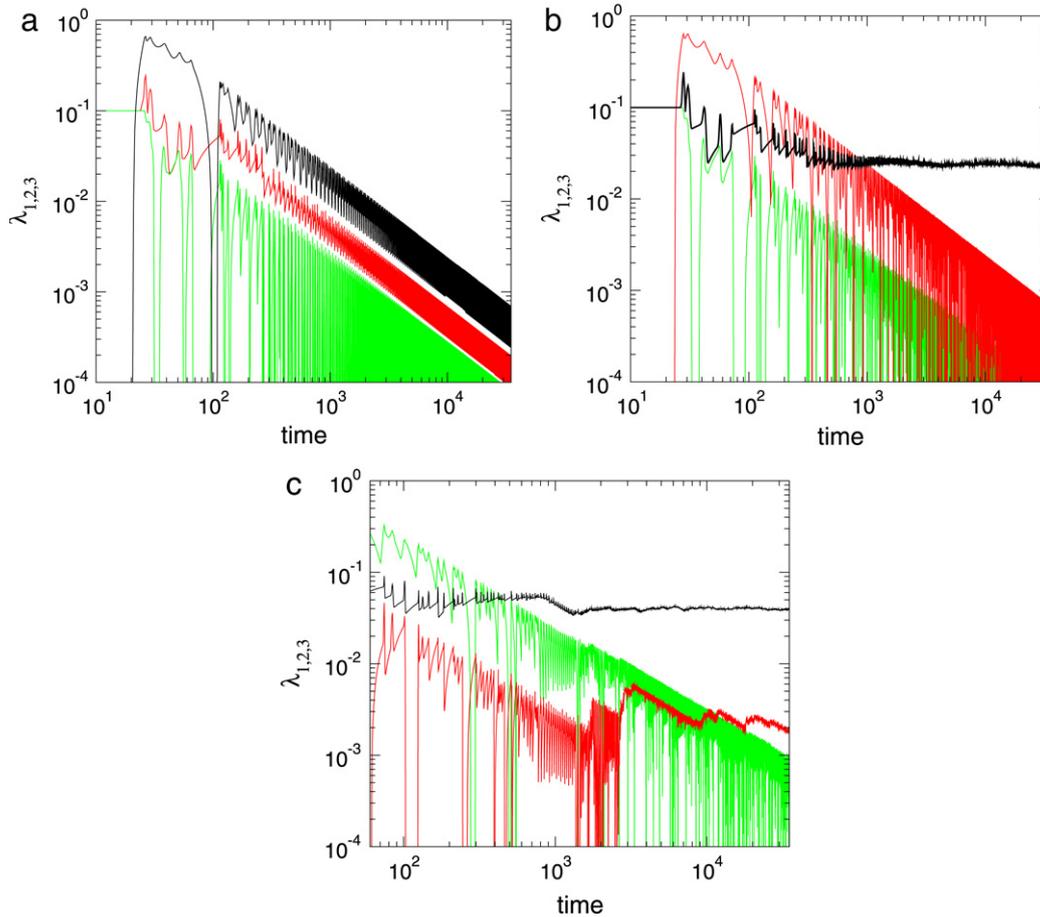
Fig. 7. (color online) Time evolution of the three largest Lyapunov exponents of the dynamical system formed by *N* Fourier modes. The parameters are the same as in Fig. 5.

alternates from a quiescent pre-bifurcation state to a bursting post-bifurcation one. In our system we conjecture that, for that transition to occur, a low-period unstable periodic orbit must lose transversal stability through a bifurcation [34]. Due to the intrinsic randomness characteristic of the chaotic dynamics (in the homogeneous manifold) the transversal dynamics is chaotically driven so that the system undergoes fluctuations to-and-fro the bifurcation point.

We remark, however, that the existence of an on–off bifurcation is quite typical for our system, as illustrated by Fig. 8(b), where the statistical signature of 3/2-power law scaling is obtained with two widely different values of ν. Actually for all values of ν we have considered this transition has been verified. The difference we observed among different values of ν was in the average inter-spike interval

$$\bar{\tau} = \frac{\int_0^\infty P(\tau)\tau d\tau}{\int_0^\infty P(\tau)d\tau}, \tag{17}$$

as illustrated by Fig. 8(c), where we plot $\bar{\tau}$ as a function of $|\nu - \nu^*|$, where $\nu^* = -3.515811$ is the beginning of the wide periodic window in the bifurcation diagram of Fig. 6. Similar results were obtained for other values of ν^* corresponding to other periodic windows. The closer we are from ν^* the larger is the interspike interval, what is consistent with the fact that there are no spatial mode excitation if ν is chosen inside a given periodic window (i.e. the inter-spike interval would go to infinity if we approach ν^* from less values). In fact, the numerical results for this (and other windows, not shown here) reveal a power-law scaling

$$\bar{\tau} \sim |\nu - \nu^*|^{-\varpi}, \tag{18}$$

where $\varpi = 0.78 \pm 0.01$. Using the terminology of on–off intermittency, the interspike interval would be equivalent to the laminar time. Although there are no general results on the scaling of the mean laminar time near the onset of on–off intermittency, there are numerical evidences that for one-dimensional maps with uniform random driving this exponent is $\varpi = 1$ [32].

The existence of a bubbling transition associated with the nonlinear excitation of spatial modes reveal many interesting features underlying the system dynamics. First recall that a chaotic orbit must exist in the homogeneous manifold so as to pump energy to the spatial modes to be excited. When this occurs, it means that some unstable periodic orbit embedded in the chaotic orbit in $\mathcal{M}$ loses transversal stability, as discussed in the previous Section. However, since there is a bubbling transition, a bursting trajectory returns to the vicinity of $\mathcal{M}$. This means that the chaotic orbit itself in the homogeneous manifold remains transversely stable [16].

6. Diffusion-limited spatial mode excitation

One of the key issues involved in the process of more developed turbulence is the redistribution of energy among the modes, from those with lower to the higher κ-value. This energy redistribution is apparent when one considers the spectral mean defined as [23]

$$\sqrt{\langle N^2 \rangle} = \sqrt{\frac{\sum_{n=1}^{N}\sum_{\alpha=1}^{3} n^2 |a_{\alpha,n}|^2}{\sum_{n=1}^{N}\sum_{\alpha=1}^{3} |a_{\alpha,n}|^2}}. \tag{19}$$
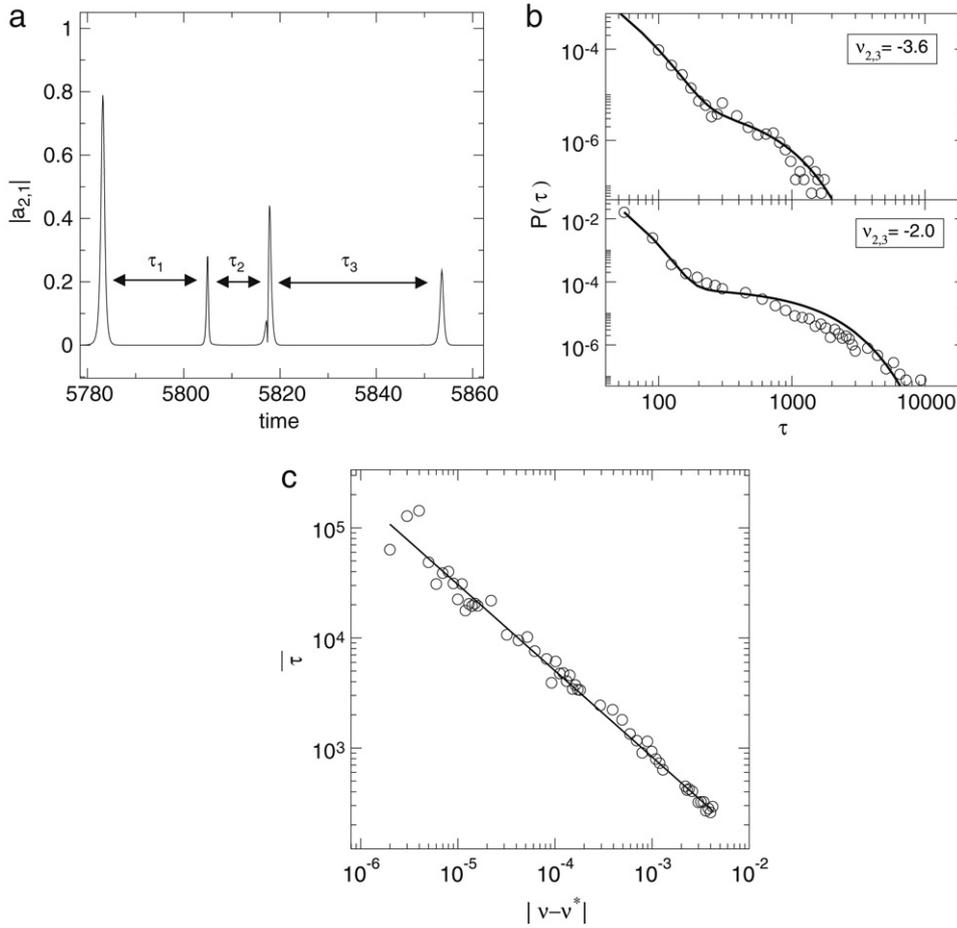
Fig. 8. (a) Time evolution of a spatial Fourier mode amplitude for $\nu_{2,3} = -3.6$. (b) Probability distribution for the duration of inter-spike intervals for $\nu_{2,3} = -3.6 < \nu^*$ and $\nu_{2,3} = -2.0 < \nu_{CR}$. The solid lines are fitting curves given by Eq. (16). (c) Average inter-spike interval as a function of the difference $|\nu - \nu^*|$, where $\nu = \nu_{2,3}$ and $\nu^* = -3.515811$ marks the beginning of a periodic window in the bifurcation diagram of Fig. 6.

The numerical experiments described in the previous section used a modest number of Fourier modes ($N = 32$). An immediate question is whether or not a larger number of modes would influence qualitatively the redistribution of the energy from temporal degrees of freedom (in the homogeneous manifold) to spatial modes. In Fig. 9(a) and (b) we plot the time evolution of the spectral mean for $N = 32$ and $N = 256$ Fourier modes, respectively, not revealing qualitative differences. This conclusion also holds for the transition to spatio-temporal chaos.

The insensitiveness of numerical results to the number of Fourier modes is not surprising since, near the onset of weak turbulence, the wave energy, formerly restricted to the homogeneous manifold, is first transferred to the lowest spatial modes. This scenario, however, is expected to change as we move towards a fully turbulent case, where the strong interaction there existing among different spatial scales leads to a fast redistribution of the wave energy to the lowest wavelengths, such that the use of a large number N of modes would be necessary.

The time evolution of the above spectral mean is plotted in Fig. 9 for 32 and 256 modes. As stated above, although the evolution for both number of modes would show small quantitative differences, the general trend is the same, namely a bubbling behavior with small quiescent intervals interspersed with peaks. The latter peaks correspond just to the epochs during which energy from the chaotic dynamics on the homogeneous subspace is imparted to spatial modes, corresponding to a redistribution of energy which occurs in a spike-like manner. Since the exact time at which these spikes occur is immaterial, for one is interested in statistical
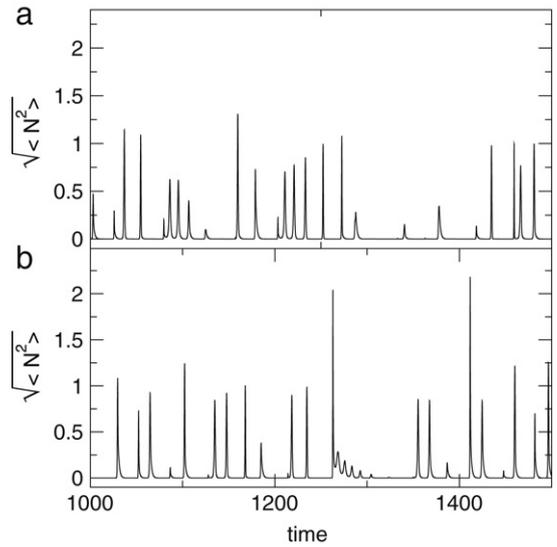

Fig. 9. Time evolution of the spectral mean for (a) $N = 32$; (b) $N = 256$ Fourier modes. Other parameters are $D = 1.0$, $\nu_1 = 0.1$, and $\nu_{2,3} = -4.5$.

averages, we may well use a smaller number of modes ($N = 32$ has been our choice) in order to get faster results. We stress, however, that this freedom is only possible near the onset of spatio-temporal chaos, where the number of spatial modes excited is rather limited.
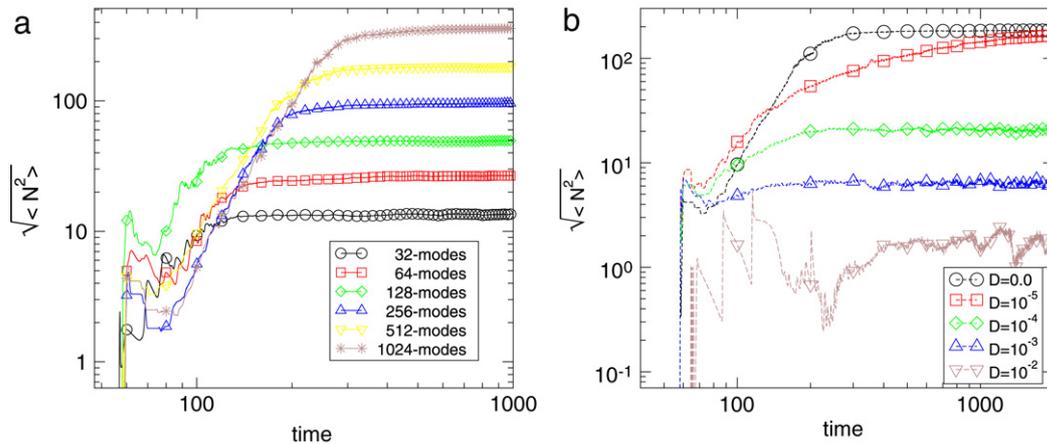
Fig. 10. (color online) Spectral mean as a function of time for (a) various numbers of modes in Fourier space, with $D = 0$, and (b) different values of the diffusion coefficient. We used $\nu_1 = 0.1$ and $\nu_{2,3} = -4.5$.

As we progress towards fully-developed spatio-temporal chaos, more and more Fourier modes would be needed to describe the energy flow from larger to smaller scales.

Another comparison of this kind is shown in Fig. 10(a), where the time evolution of $\sqrt{\langle N^2 \rangle}$ is followed in its beginning for various numbers of Fourier modes, and without spatial diffusion ($D = 0$). As a general trend, over the first hundred iterations the spectral mean increases slowly to a saturation value of a fraction (roughly one third) of the number of modes itself. This means that energy is pumped from the purely temporal mode to the spatial modes up to a saturating number of modes.

It turns out that the saturating number of modes is limited by the spatial diffusion, as illustrated by Fig. 10(b), where the time evolution of the spectral mean is followed for different values of the diffusion coefficient, at a fixed number of Fourier modes. The saturating number of modes decreases as diffusion becomes stronger, i.e. higher values of D are considered. However, if D is too large the spectral mean does not seem to saturate, rather fluctuating around a bounded value.

The overall aspects of the diffusion effect on the spatial mode excitation can be understood by a simple linear analysis of Eq. (7). If the wave amplitudes are small enough we can neglect the quadratic nonlinearity and suppose a linear solution of the form $A_1(x, t) \sim A_{10}(t)e^{ik_1 x}$. Substituting into (7) gives the linear equation

$$\frac{dA_{10}}{dt} \approx \left(\nu_1 - k_1^2 D - ik_1 v_{g1} \right) A_{10}. \tag{20}$$

The term within parentheses, which is the effective growth rate/decay of the (real) mode amplitude, decreases as D is augmented, what explains why diffusion limits the excitation of spatial modes. Neglecting the group velocity of the wave, for not being relevant in the present crude approximation, diffusion affects more the modes with wave number smaller than

$$k_{CR} = \sqrt{\frac{\nu_1}{D}}. \tag{21}$$

In order to investigate the limit of applicability of the linear approximation we have made the following numerical experiment: for a given value of the diffusion coefficient D we have analyzed the dependence of the real amplitude of the mode $|A_1|$ on the number of Fourier modes retained N. We observed that this amplitude decays with N, and we computed for what N^* this amplitude is less or equal to a specified small threshold (of about 0.005). The critical wave number k_{CR} is taken to be the closest
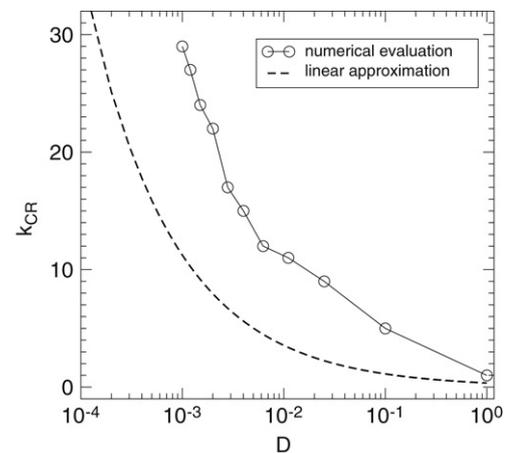

Fig. 11. Critical wave number as a function of the the diffusion coefficient, for $\nu_1 = 0.1$, $\nu_{2,3} = -4.5$, and $N = 256$ Fourier modes, assuming a tolerance of 0.005 (see text). The dashed line represents the result of a linearized theory, Eq. (21).

integer corresponding to N^* (for example, if N^* corresponds to $k = 10$, then $k_{CR} = 9$ and so on).

Fig. 11 shows the dependence of the critical value k_{CR} on the diffusion coefficient D. We also plotted the result which comes linear approximation, Eq. (21), for comparison. The overall behavior of the critical k is the same as predicted by linear theory, i.e. the less the diffusion coefficient, the greater is the critical wave number excited, the discrepancies being naturally an effect of the nonlinearity of the system. Moreover, for large D the numerical result tends to the prediction of the linear theory, what is consistent with the observation that, in the limit of strong diffusion, the nonlinear terms relax very fast. We remark, however, that even a linear analysis will fail if the dynamics in the homogeneous manifold is periodic (see the inset of Fig. 6(a) and (b) for a representative example).

7. Conclusions

In this paper we proposed a scenario for explaining the onset of spatio-temporal chaos in spatially extended systems by the nonlinear excitation of spatial modes powered by the chaotic dynamics in a low-dimensional and spatially homogeneous attractor. In mathematical terms, there must be an invariant subspace (embedded in the system phase space) containing a chaotic attractor with pure temporal chaos, i.e. no spatial modes. Energy is pumped from this chaotic state to excite inhomogeneous spatial modes.

The onset of spatio-temporal chaos occurs when some unstable periodic orbit, embedded in the spatially homogeneous chaotic attractor, loses transversal stability (with respect to the homogeneous subspace). Although all the infinitely many preimages of this (supposedly low-period) unstable periodic orbit also lose transversal stability, the set of all such orbits have Lebesgue measure zero. The full measure of the attractor is thus supported by transversely stable orbits.

In spite of this, such transversely orbits have a pronounced effect on the dynamics of a trajectory off but near this homogeneous subspace. During various periods of time such trajectory wanders in the immediate vicinity of the homogeneous state, making for a spatially quiescent state. As the trajectory approaches a transversely unstable orbit, it departs from the homogeneous state in a burst-like fashion, exciting spatial modes. Due to the prevalence of the transversely stable orbits, however, the trajectory comes back to the neighborhood of the homogeneous state. This bubbling behavior belongs to the same category of the on–off intermittency, with the same statistical properties in the vicinity of the transition.

When spatial modes are excited, the energy related to the spatially homogeneous (and chaotic) state is redistributed through this bubbling mechanism. Since the latter is markedly nonuniform, we expect equipartition of energy to be severely broken just after the onset of spatio-temporal chaos. This is not surprising, though, since equipartition of energy is related to ergodic behavior in both spatial and temporal scales, a condition only feasible in fully-developed spatio-temporal chaos.

We have used a linear approach to derive a condition under which this redistribution of energy is limited by diffusive effects. Energy is distributed over a saturate number of modes, the value of which depends on the diffusion coefficient. In particular, diffusion limits more those modes with larger wave numbers. We have used, as a model system, the nonlinear interaction of two dispersive waves in one direction. However, since the assumptions we have used are rather general, the scenario for the onset of spatio-temporal chaos we have described in this paper hold for a large variety of other spatially extended dynamical systems as well.

Our description might be regarded as a scenario for the onset of turbulence in fluid systems, provided some pre-conditions are fulfilled: (i) the properties of interest in the continuous system are adequately emulated by a discrete lattice system. Some categories of wave propagation, for example, fit into this description; (ii) there must exist a temporally chaotic but spatially homogeneous state from which the system draws energy to nonlinearly excite spatial modes. A well-known example of such spatially homogeneous state is the completely synchronized state of an ensemble of chaotic oscillators. In a certain extent, our system belongs to this class, since the modes in Fourier space could be regarded as coupled oscillators undergoing chaotic evolution. Finally (iii) there must exists unstable states embedded in the chaotic attractor which can lose transversal stability. The latter seems to be the hardest condition to warrant in a practical system. Some hints could be given by the statistical properties of the finite-time Lyapunov exponents.

References

[1] U. Frisch, Turbulence: The Legacy of A. N. Kolmogorov, CUP, Cambridge, 1995.
[2] A.N. Kolmogorov, Dokl. Akad. Nauk USSR 30 (4) (1941). An English translation is available in Proc. R. Soc. Lond. A 434, 9 (1991).
[3] L.D. Landau, E.M. Lifshitz, Fluid Mechanics, 2nd edition, Pergamon Press, New York, 1987.
[4] D. Ruelle, F. Takens, Commun. Math. Phys. 20 (1971) 167;
    S. Newhouse, D. Ruelle, F. Takens, Commun. Math. Phys. 64 (1978) 35.
[5] J.P. Gollub, H.L. Swinney, Phys. Rev. Lett. 35 (1975) 927;
    T. Klinger, et al., Phys. Rev. Lett. 79 (1997) 3913;
    A. Cumming, P.S. Linsay, Phys. Rev. Lett. 60 (1988) 2719.
[6] R.W. Walden, P. Kolodner, A. Passner, C.M. Surko, Phys. Rev. Lett. 53 (1984) 242.
[7] P. Manneville, Instabilities, Chaos And Turbulence: An Introduction To Nonlinear Dynamics And Complex Systems, Imperial College Press, London, 2004.
[8] E. Ott, Chaos in Dynamical Systems, 2nd edition, Cambridge University Press, Cambridge, 2002.
[9] B.W. Zeff, et al., Nature (London) 421 (2003) 146;
    Y. Li, C. Meneveau, Phys. Rev. Lett. 95 (2005) 164502;
    E.L. Rempel, A.C.-L. Chian, Phys. Rev. Lett. 98 (2007) 014101.
[10] The definition of spatio-temporal chaos has been put in a rigorous basis in many papers as L.A. Bunimovich, Ya.G. Sinai, Nonlinearity 1 (1988) 491;
    J. Bricmont, A. Kupiainen, Physica D 103 (1997) 18;
    M. Jiang, Y.B. Pesin, Commun. Math. Phys. 193 (1998) 675.
[11] G. Corso, A.J. Lichtenberg, Phys. Rev. E 59 (1999) 6652.
[12] B. Fornberg, A Practical Guide to Pseudospectral Methods, Cambridge University Press, Cambridge, 1996.
[13] J.C.P. Coninck, S.R. Lopes, R.L. Viana, Phys. Rev. E 70 (2004) 56403; Physica A 343 (2004) 247.
[14] K. He, A.C.-L. Chian, Phys. Rev. Lett. 91 (2003) 034102;
    K. He, Phys. Rev. Lett. 94 (2005) 034101.
[15] C. Grebogi, E. Ott, J.A. Yorke, Phys. Rev. A 37 (1988) 1711.
[16] R.L. Viana, C. Grebogi, S.E. de, S. Pinto, S.R. Lopes, A.M. Batista, J. Kurths, Physica D 206 (2005) 94.
[17] P. Ashwin, J. Buescu, I. Stewart, Phys. Lett. A 193 (1994) 126;
    S.C. Venkataramani, B.R. Hunt, E. Ott, D.J. Gauthier, J.C. Bienfang, Phys. Rev. Lett. 77 (1996) 5361;
    S.C. Venkataramani, B.R. Hunt, E. Ott, Phys. Rev. E 54 (1996) 1346.
[18] L. Turner, Phys. Rev. E 54 (1996) 5822;
    Y.C. Li, Internat. J. Bifur. Chaos 17 (2007) 85.
[19] A.C.-L. Chian, S.R. Lopes, M.V. Alves, Astron. Astrophys. 290 (1994) L13;
    A.C.-L. Chian, F.B. Rizzato, J. Plasmas Phys. 51 (1994) 61.
[20] A. Rundquist, et al., Science 280 (1998) 1412;
    G.I. Stegeman, M. Segev, Science 286 (1999) 1518;
    A. Picozzi, M. Haeltermann, Phys. Rev. Lett. 86 (2001) 2010.
[21] D.J. Kaup, A. Reiman, A. Bers, Rev. Mod. Phys. 51 (1979) 275.
[22] C.C. Chow, A. Bers, A.K. Ram, Phys. Rev. Lett. 68 (1992) 3379.
[23] S.R. Lopes, F.B. Rizzato, Phys. Rev. E 60 (1999) 5375.
[24] M. Frichembruder, R. Pakter, F.B. Rizzato, Physica D 215 (2006) 99.
[25] J.D. Szezech Jr., S.R. Lopes, R.L. Viana, Phys. Rev. E 75 (2007) 67202.
[26] A.M. Batista, I.L. Caldas, S.R. Lopes, R.L. Viana, W. Horton, P.J. Morrison, Phys. Plasmas 13 (2006) 42510.
[27] K. Josic, Phys. Rev. Lett. 80 (1998) 3053.
[28] A.V. Zimin, B.R. Hunt, E. Ott, Phys. Rev. E 67 (2003) 16204.
[29] Y. Kuramoto, Chemical Oscillations, Waves, and Turbulence, Springer Verlag, Berlin, 1984.
[30] A. Wolf, J.B. Swift, H.L. Swinney, J.A. Vastano, Physica D 16 (1985) 285;
    M. Yamada, K. Ohkitani, Phys. Rev. Lett. 60 (1988) 983.
[31] E. Covas, P. Ashwin, R. Tavakol, Phys. Rev. E 56 (1997) 6451.
[32] N. Platt, E.A. Spiegel, C. Tresser, Phys. Rev. Lett. 70 (1993) 279;
    J.F. Heagy, N. Platt, S.M. Hammel, Phys. Rev. E 49 (1994) 1140.
[33] N. Platt, S.M. Hammel, J.F. Heagy, Phys. Rev. Lett. 72 (1994) 3498.
[34] B.R. Hunt, E. Ott, Phys. Rev. E 54 (1996) 328.